

# FINER-SCALE MONITORING AND ANALYSIS OF 2016–2021 DUST STORMS DISASTERS IN CHINA BASED ON HIMAWARI-8 SATELLITE IMAGERIES

Ming Chen<sup>1</sup>, Nana Luo<sup>1</sup>, Mingyi Du<sup>1,\*</sup>

<sup>1</sup> School of Geomatics and Urban Spatial Information, Beijing University of Civil Engineering and Architecture, Beijing, 102616, China, 2108570021060@stu.bucea.edu.cn (M. Chen), luonana@bucea.edu.cn (N. L), dumingyi@bucea.edu.cn (M. Du).

**KEY WORDS:** Himawari-8, Dust Storm, Classification, Near Real-time Detection, Analysis.

## ABSTRACT:

Today, remote sensing is one of the important techniques for natural disasters monitoring. Using the Himawari-8 new generation of geostationary meteorological satellite image data, we identified and monitored 2016-2021 dust storm disasters in China at the finer scale, and compared the object-oriented classification, supervised and unsupervised classification methods. Taking the dust storm on May 5, 2016 as example, the average accuracy and kappa coefficient of the supervised classification were 0.78 and 0.68, while the object-oriented classification were 0.81, 0.73. We used the object-oriented classification method to classify the 2016-2021 dust storm incidents across China. In 2021, the largest area affected by sandstorms was about 68.33km<sup>2</sup>, the smallest area was about 2.08km<sup>2</sup>, and the average area was about 22.25km<sup>2</sup>. During 2016-2021, the most severe and wide-spreading sandstorm occurred on March 14-18 2021. The dust storm first appeared in northwestern Mongolia on March 14, and then spread southeast to China. The dust area covered Beijing on the 15th, and then spread from eastern China to the western regions of North China and Northeast China, including most of the Hexi Corridor. On the 16th and 17th, the influence of the dust storms narrowed to central and western Inner Mongolia, northern Gansu and southern Mongolia. The dust storm gradually disappeared on the 18th.

## 1. INTRODUCTION

Every year, various natural disasters cause incalculable economic losses in China, and the infrastructure is seriously damaged and the ecological environment and public safety are endangered (Wang and Liu, 2015). With the continuous development of remote sensing technology, the spatial and temporal resolution of satellite images was getting higher and higher, and the data collection capabilities of various sensors was continuously improved, making remote sensing one of the important monitoring technology methods for natural disasters, and playing an important role in decision-making applications such as disaster early warning, loss monitoring, and post disaster reconstruction (Han et al., 2021). Polar-orbiting satellites and geostationary orbit satellites are the main remote sensing methods, with a wide range of monitoring range and strong observation capabilities, which can carry out near-real-time all-weather monitoring and early warning of large-scale disaster environments, scopes, changes, etc. Through remote sensing disaster monitoring, information can be obtained quickly and accurately, including a series of data before and after disasters, which is the guarantee and foundation for disaster prevention and control. The application of remote sensing monitoring methods and the construction of a systematic disaster monitoring method are necessary requirements for scientific and efficient disaster prevention and control (Twumasi et al., 2019).

The ongoing sandstorm events have had a clear and far-reaching impact on global ecosystems and socio-economies. China is one of the major countries in the world with frequent dust storms at an average of 15.7 incidents in 2000-2010, 8.8 incidents in 2011-2014, and 13.2 incidents in 2015-2019 (Zhang, 2018). Especially, March 15, 2021 experienced the most intense sandstorm across the county in the last decade. The impacts of

dust storms are significant. It is estimated that the March 15, 2021 sandstorm affected about 466,000 km<sup>2</sup> area. It not only increases the concentrations of particulate matters making the public more susceptible to illness, reduces air quality and damages the ecological environment, but also affects industrial and agricultural production as well as visibility and traffic safety (Muhammad et al., 2012). These economic and environmental impacts also threaten peoples' well-being (Liu, 2018), and accelerate soil desertification (Yang et al., 2018).

Traditional methods for dust storm monitoring include ground stations and satellite retrieval. Ground-level measures such as watchtowers, video surveillance, and perception information are limited to land, and difficult to identify large-scale and long-distance dust transmission (Zhang, 2018). A few studies use fine-mode ground-measured aerosol to identify dust storm (Ke et al., 2020). Satellite remote sensing has great potential advantages in both temporal and spatial scale monitoring. In particular, with public, finer-scale remote sensing images, monitoring dust storms has received growing attentions. Such data also enables extensive monitoring of dust events as well as transmissions on a global scale. Many satellite-based dust identification algorithms have been proposed based on spectral characteristics of dust particles in visible light, near-infrared, thermal infrared bands (Luo et al., 2015; Zhang et al., 2018). However, comprehensive interpretation of sand-dust events is missing, and near-dynamic and real-time monitoring is quite few.

Different identification algorithms were proposed to evaluate the monitoring results of dust and compare them with the ground measurement results. Spatial analysis and statistical methods were used to analyze the temporal and spatial distribution characteristics and trends of sand dust, so as to

\* Corresponding author

provide basis for sand dust control, environmental assessment and avoiding other possible climate risks. Therefore, real-time monitoring dust storm events and analyzing the temporal and spatial variation characteristics is important. It also plays an important role in sandstorm disaster prediction and warning, as well as improving the quality of peoples' life and mitigating global climate degradation.

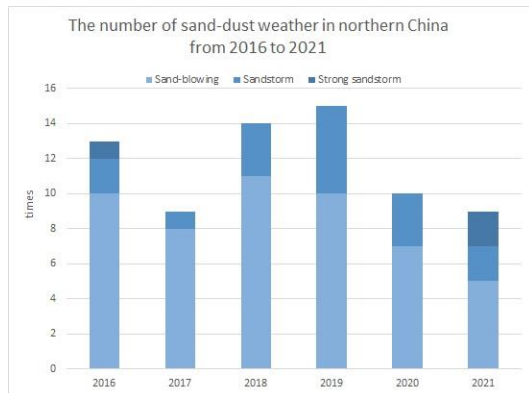


**Figure 1.** The number of sand-dust weather in northern China from 2016 to 2021

## 2. RELATED WORK

Traditional remote sensing image classification methods, such as supervised classification, can easily lead to a reduction in classification accuracy, a large amount of redundancy in spatial data and a waste of resources. The object-oriented classification method appears to solve these problems. Baatz et al. first proposed a multi-scale segmentation algorithm, which laid the foundation for object-oriented image classification (Baatz et al., 2000). With the continuous development of high-resolution remote sensing images, the object-oriented classification method has been gradually improved. Based on the particularity of the study area, Qiao Yuexia et al. proposed a classification method combining object-oriented technology and multi-temporal remote sensing data, and proposed the difference of seasonal vegetation index difference. And she also proposed the concept of assisting in the classification of forest land types (Qiao et al., 2017). Sun Mengdi extracted wetland information in the Dulbert area through a classification method combining object-oriented and visual interpretation. On the basis of the classification results, statistical analysis methods such as transition matrix were used to study the wetland area and temporal and spatial changes in the study area (Sun, 2017). Feng Chao et al. adopted the object-oriented method, based on the texture and spectral characteristics of the ground object types on the image, and used the ENVI object-oriented feature extraction module to classify the SPOT5 images of the test road area, so as to quantitatively and dynamically analyse the changes of the ground object types (Feng et al., 2016). Huang Chao et al. used the West Lake area of Hangzhou to extract green space information, and the results showed that the accuracy of object-oriented classification was better than supervised classification in this data (Huang et al., 2016). Taking TM images as an example, Cui et al. conducted experiments on the object-oriented classification method and the pixel-based classification method based on various features, and compared and analysed the classification accuracy. The experiments showed that the object-oriented classification method has higher accuracy (Cui et al., 2008).

At present, the object-oriented image classification focuses more on land use classification and forest classification. Land use classification mainly studies the types of natural and artificial covers. The commonly used method is to extract the feature information of different objects through rules or classification algorithms and then classify them. In this paper, the object-oriented method is used to classify the H-8 remote sensing images, so as to achieve the purpose of extracting sandstorms. Combined with the high temporal resolution of the H-8 images, the sand dust can be monitored in near real time.

## 3. MATERIALS

### 3.1 Study Area

Our research area basically covers the whole territory of China, from 80°0' to 135°3'E, and from 2°50' to 53°57'N (Fig. 2). The northern part of the study area is mostly arid and semi-arid, with low average annual precipitation. It includes the Gobi and deserts, such as the Taklamakan Desert and the Badain Jaran Desert, which provides sufficient sources of sand and dust for the occurrence of sand and dust events (Kurosaki et al., 2011).

### 3.2 Data Sets

Himawari-8(H8) meteorological satellite is one of the himawari series satellites designed and manufactured by Japan Aerospace Exploration Agency(JAXA). It weighs about 3500 kg and has a design life of more than 15 years. The satellite was successfully launched by H2A rocket on October 7, 2014, and began operation on July 7, 2015. It is equipped with Advanced Himawari Imager (AHI). It can provide multi spectral images, which are mainly used to monitor storm clouds, typhoon movements, volcanoes with continuous eruptions and other disaster prevention fields.

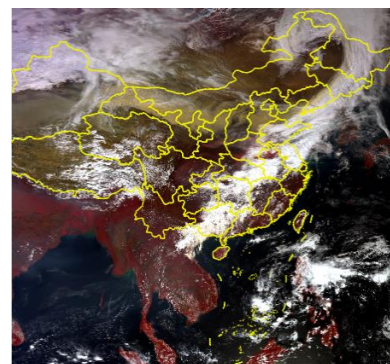


**Figure 2.** Study area (Himawari-8 geostationary meteorological satellite false color image)

As is shown in Table 1, the AHI has 16 channels, including three visible light channels, three near-infrared channels and ten mid infrared and thermal infrared channels. The spatial resolution of visible light is 0.5 km to 1 km, and the spatial resolution of infrared is 1 km to 2 km. AHI can scan the full disk in 10 minutes. The data are from the Earth Observation Research Center (EORC) of Japan Aerospace Exploration Agency and provided by the Japan Meteorological Agency(JMA) (download from the website <https://www.eorc.jaxa.jp/ptree/index.html>).

**Table 1.** Advanced Himawari Imager (AHI) Channels

| Channel Name | Category      | Central Wavelength( $\mu\text{m}$ ) | Spatial Resolution(km) |
|--------------|---------------|-------------------------------------|------------------------|
| albedo_01    | Visible light | 0.47                                | 1.0                    |
| albedo_02    | Visible light | 0.51                                | 1.0                    |
| albedo_03    | Visible light | 0.64                                | 0.5                    |
| albedo_04    | Near infrared | 0.86                                | 1.0                    |
| albedo_05    | Near infrared | 1.6                                 | 2.0                    |
| albedo_06    | Near infrared | 2.3                                 | 2.0                    |
| tbb_07       | Shortwave     | 3.9                                 | 2.0                    |
| tbb_08       | Infrared      | 6.2                                 | 2.0                    |
| tbb_09       | Water vapor   | 6.9                                 | 2.0                    |
| tbb_10       | Water vapor   | 7.3                                 | 2.0                    |
| tbb_11       | Water vapor   | 8.6                                 | 2.0                    |
| tbb_12       | Infrared      | 9.6                                 | 2.0                    |
| tbb_13       | Infrared      | 10.4                                | 2.0                    |
| tbb_14       | Infrared      | 11.2                                | 2.0                    |
| tbb_15       | Infrared      | 12.4                                | 2.0                    |
| tbb_16       | Infrared      | 13.3                                | 2.0                    |

### 3.3 Data Preprocessing

Geometric distortion will bring errors to the quantitative analysis, change detection, image fusion, map measurement or update processing based on remote sensing images, so it is necessary to perform geometric correction for the geometric distortion of the image. Geometric correction with known geometric information is generally implemented through Input Geometry files (Input Geometry, IGM) and Geographic Lookup Table files (GLT). The H-8 image used in this paper completely covers the study area, and only the final image of the study area is obtained by cropping.

## 4. METHODS

### 4.1 The Unsupervised Classification

Unsupervised classification (Zhang et al., 2019) is the process of searching and defining natural similar spectral clusters in multispectral images. It does not need to acquire prior knowledge of image features, only relies on the spectral information of different features on the image to extract features, achieves the purpose of classification in the difference of statistical features, and finally confirms the actual attributes of each category.

Iterative Selforganizing Data Analysis Techniques Algorithm is a repeated self-organizing data analysis technology. It calculates the class mean value uniformly distributed in the data space, and then iteratively aggregates the remaining pixels with the minimum distance technology. Each iteration recalculates the mean value, and classifies the pixels according to the new mean value.

### 4.2 The Supervised Classification

Supervised classification (Abbas et al., 2020) is a kind of remote sensing image classification, which uses the sample pixels of the confirmed category to identify other unknown category pixels. The sample pixels of the confirmed category refer to those located in the training area. In this classification, the analyst selects a certain number of training areas for each category on the image, the computer calculates statistics or other information for each training sample area, compares each pixel with the training sample, and divides it into the most

similar sample classes according to different rules. The selected sample area is required to be typical and representative. If the criterion meets the requirements of classification accuracy, the criterion is established; On the contrary, the decision rules of classification need to be re-established until the classification accuracy requirements are met. Commonly used algorithms are discriminant analysis, maximum likelihood analysis, feature analysis, sequential analysis and graphic recognition.

Maximum likelihood classification is one of the most commonly used supervised classification methods in image processing (Wang et al., 2010). It uses the statistical characteristics of remote sensing data, assumes that the distribution functions of various types are normal distributions, and forms elliptical or ellipsoidal distributions in multivariate space. The normal distribution law is judged by the maximum likelihood discriminant rule, and the classification result with higher accuracy is obtained. Therefore, this paper selects the maximum likelihood method for comparative analysis.

### 4.3 The Object Oriented Classification

The traditional land object classification method takes the image pixel as the basic unit and uses the spectral characteristics of different land objects to classify. The object-oriented classification method takes the homogeneous object obtained after image segmentation as the basic unit of classification, and combines the spectral information of the pixel with the spatial features between adjacent areas. Some pixels are integrated into one object after segmentation, which not only reduces the amount of data but also ensures the integrity of the original data information.

The object-oriented classification methods include rule-based classification, such as threshold classification, membership function classification, etc.; there are also sample-based supervised classification, such as support vector machine classification, nearest neighbor classification, decision tree classification and random forest classification. In the sample-based supervised classification, the classification results will be directly affected by the classification algorithm. In order to eliminate the influence of the accuracy evaluation bias caused by a single classifier, this paper mainly studied the sample-based supervised classification method, and adopted the method

of membership classification to classify the object-oriented H-8 image, the flowchart is shown in Fig 3.

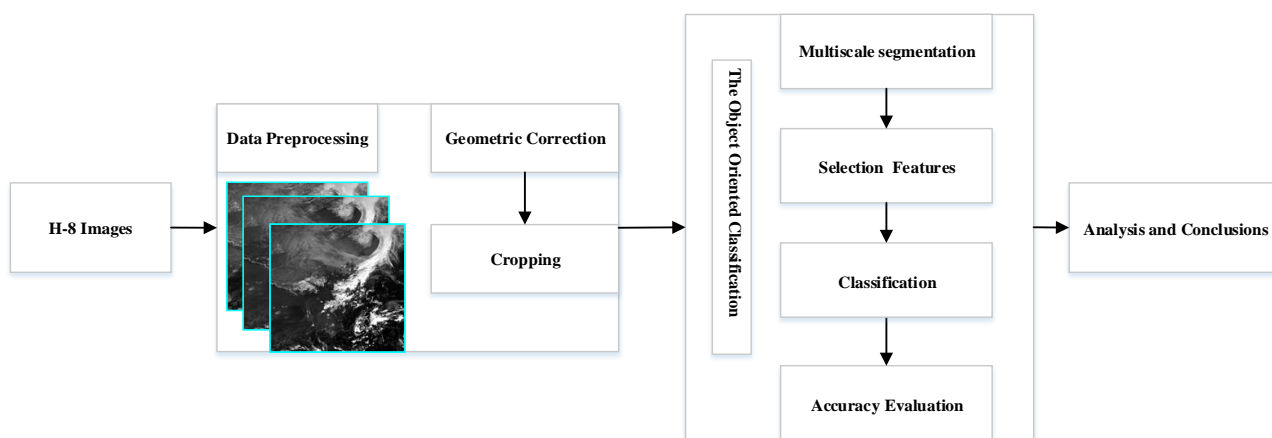


Figure 3. Flow chart of object-oriented classification processing

#### 4.3.1 Optimal Segmentation Scale

Image segmentation is the first and most important step in information interpretation. Therefore, the basis of subsequent information extraction and classification, the selection of segmentation scale is the difficulty of image segmentation. Image segmentation refers to using the shape, spectrum, texture and other information of the pixel to comprehensively calculate the comprehensive eigenvalues of the spectrum and shape heterogeneity factor of each pixel according to certain rules, and divide the image into regions with similar attributes according to the features. At present, the commonly used methods for selecting the optimal scale include trial and error method, local variance method, variogram method, objective function method, RMA method, maximum area method, scale comparison method and object matching method, etc, each method has its advantages and disadvantages.

The selection of the optimal scale is a complex and changeable process (Wang and Liu, 2015). Different choices need to be made according to different situations. Although there are many quantitative analysis methods, most of them are too complicated and have too many calculation parameters. Therefore, continuous experiments are carried out. Comparison to select the optimal scale in the subjective sense is still a common method. In this paper, the optimal segmentation scale is determined by trial and error method.

#### 4.3.2 Selection of Classification Features

The segmented objects have a variety of features: spectral features, texture features, geometric features, etc. Through the statistics and analysis of the characteristics of each object, the objects with similar characteristics are divided into one category, and the key to distinguish one category of objects from another category is to find suitable features. The feature attributes of the segmented objects reflect the relevant information of the actual objects, and it is the main basis for information extraction and classification. Because the object is composed of several pixels, the characteristics of the entire object can be calculated according to the feature information of each pixel in the object and the relationship between the pixels. The classification features selected in this study include Mean, Brightness, Length/Width, Width, Shape index.

#### 4.3.3 Accuracy Evaluation

The quality of remote sensing image classification results needs to be quantitatively evaluated with accuracy. The accuracy of the objects in the classified images and their corresponding actual objects are compared with each other, and the classification accuracy of each class is represented by the proportion of correct classification. This paper uses random sample points for testing, and uses four evaluation indicators in the confusion matrix to evaluate the classification results, namely: evaluating the user accuracy and mapping accuracy of a single category; evaluating the overall classification accuracy and kappa coefficient.

The overall classification accuracy is equal to the sum of correctly classified cells divided by the total number of cells. The number of correctly classified cells is distributed along the diagonal of the confusion matrix, and the total number of cells is equal to the total number of cells in all true reference sources.

The kappa coefficient is calculated by multiplying the total number of pixels of all true references (N) by the sum of the diagonals of the confusion matrix ( $\sum_k X_{kk}$ ) and subtracting the sum of the number of true reference pixels in a class and the total number of classified pixels in that class after the product is summed for all categories, it is divided by the square of the total number of pixels minus the product of the total number of true reference pixels in a category and the total number of classified pixels in that category. The result of summing all categories. The formula (1) for calculating the kappa coefficient is as follows:

$$K = \frac{N \sum_k X_{kk} - \sum_k X_{k.} X_{.k}}{N^2 - \sum_k X_{k.} X_{.k}}, \quad (1)$$

## 5. RESULTS

### 5.1 Results of The Unsupervised Classification

The ISODATA technique in unsupervised classification was used to identify sand and dust. From the extraction results in Figure 4, it can be seen that the sand dust were shown as red patches, and the identification was relatively accurate on the whole. In some areas, clouds and land were identified as dust, and there were unidentified places.

The unsupervised classification does not need much knowledge and is realized by computer, so the error is low and the classification result is more homogeneous than supervised classification; It needs a lot of analysis to get reliable results, and it is more difficult to match because of the existence of the same object different spectrum and the foreign object same spectrum.

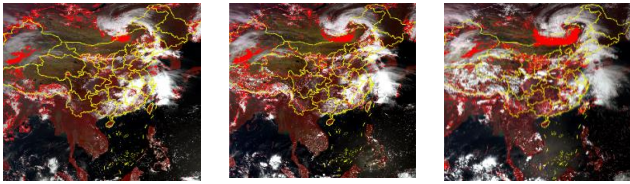


**Figure 4.** The unsupervised classification image of on May 5, 2016. From left to right, they are 3:00, 5:00, 7:00UTC.

### 5.2 Results of The Supervised Classification

From left to right in Fig 5 were the images of the supervised classification results using the maximum likelihood method at 3:00, 5:00, and 7:00UTC on May 5, 2016. By selecting appropriate and evenly distributed sample points for classification, most of the classification results were consistent with the original image, but also some land and cloud areas were mistakenly classified as dust areas.

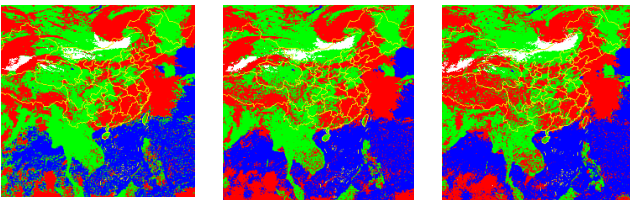


**Figure 5.** The supervised classification image of on May 5, 2016. From left to right, they are 3:00, 5:00, 7:00UTC.

Supervised classification results utilize a confusion matrix for evaluating the accuracy of feature information extraction. At 03:00, 05:00, 07:00 UTC on May 5, 2016, 190, 123, and 155 validation samples were selected on the original image, and the overall accuracy and Kappa coefficient were calculated (Table 2).

**Table 2.** The Overall Accuracy and Kappa Coefficient of the supervised classification results at 3:00, 5:00, 7:00 UTC on May 5, 2016

|           | Overall Accuracy | Kappa Coefficient |
|-----------|------------------|-------------------|
| 03:00 UTC | 0.7748           | 0.6669            |
| 05:00 UTC | 0.7942           | 0.7084            |
| 07:00 UTC | 0.7691           | 0.6711            |
| Average   | 0.7794           | 0.6821            |

### 5.3 Results of The Object Oriented Classification

The Object Oriented Classification method is obviously better than other methods mentioned. For qualitative evaluation, the object-oriented classification results of 03:00, 05:00, 07:00 UTC on May 5, 2016 were shown in Figure 6, which was a typical sandstorm event in northern China, and the white in the classified image is sand dust, which is consistent with the location of the dust area shown in the AHI image.

Accuracy evaluation is an important step in image classification. In this section, the confusion matrix was used to evaluate the accuracy of feature information extraction. At 03:00, 05:00, 07:00 UTC on May 5, 2016, 184, 228, and 181 sample verification points were selected on the original image, and the overall accuracy and Kappa coefficient were calculated (Table 3).

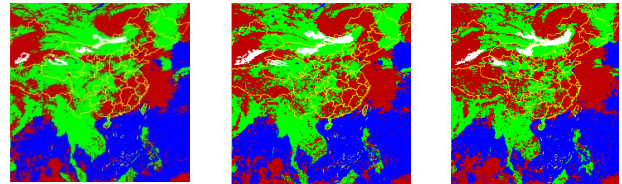


**Figure 6.** The object oriented classification image of on May 5, 2016. From left to right, they are 3:00, 5:00, 7:00UTC.

**Table 3.** The Overall Accuracy and Kappa Coefficient of the object-oriented classification results at 3:00, 5:00, 7:00 UTC on May 5, 2016

|           | Overall Accuracy | Kappa Coefficient |
|-----------|------------------|-------------------|
| 03:00 UTC | 0.8216           | 0.7314            |
| 05:00 UTC | 0.8166           | 0.7497            |
| 07:00 UTC | 0.7967           | 0.7222            |
| Average   | 0.8116           | 0.7344            |

### 5.4 A Sandstorm Incident

From March 14th to 18th, 2021, sandstorms occurred in many places in northern China. This was a sandstorm with the greatest intensity and widest range in the past 10 years. The dust storm first appeared in northwestern Mongolia at 4:10UTC on March 14, 2021, as shown in the white area in Figure 7 (upper left). The sand dust area then spread to the southeast and reached the territory of China. At 00:00 UTC on March 15, 2021, the sand dust area covered Beijing. At 04:00UTC on March 15, it spread from eastern China to the western regions of northern and northeastern China, including most of the Hexi Corridor. At 06:00UTC on March 15th, the sand and dust area continued to spread in the north-south direction, with the largest impact area.

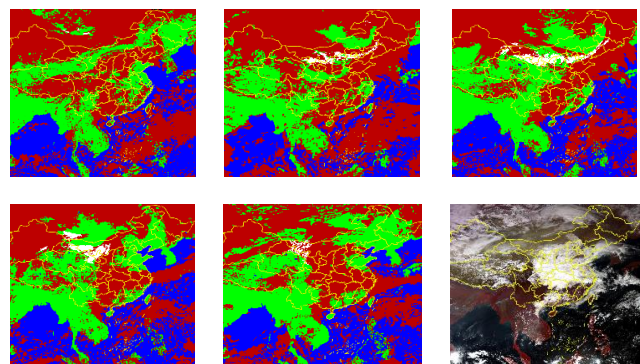


**Figure 7.** Dust area (white patch) March 14th 4:10UTC (upper left), March 15th 0:00UTC (upper middle), March 15th 4:00UTC (upper right), March 16th 4:00UTC (bottom left), March 17th 4:00UTC (bottom middle), March 18th 6:00UTC (bottom right)

At 4:00UTC on March 16, the impact of the dust storm narrowed to central and western Inner Mongolia, northern Gansu and some areas in southern Mongolia. At 4:00UTC on March 17, the scope of the sandstorm continued to decrease,

mainly affecting western Inner Mongolia and central Gansu. The dust storm gradually disappeared on March 18.

## 6. CONCLUSIONS

This paper used unsupervised, supervised, and object-oriented classification methods to classify Himawari-8 high-resolution images for the purpose of dust extraction. Taking the dust storm on May 5, 2016 as example, the average accuracy and kappa coefficient of the supervised classification were 0.78 and 0.68, while the object-oriented classification were 0.81, 0.73. The classification results of the three methods were compared, which were generally consistent with the original image, but the accuracy of the object-oriented classification was higher from the analysis results of the accuracy evaluation. The object-oriented classification was used to extract and analyze the sandstorm from March 14th to 18th, 2021, and the results show that it can better display the change of sandstorm diffusion. Although the object-oriented classification method can qualitatively display sand dust, it is difficult to quantify it, and which is necessary to use other data to assist, such as aerosols. Index methods can be added to quantify dust changes in future studies.

## REFERENCES

- Abbas Z, Jaber H S. Accuracy assessment of supervised classification methods for extraction land use maps using remote sensing and GIS techniques[C]//*IOP Conference Series: Materials Science and Engineering*. IOP Publishing, 2020, 745(1): 012166.
- Baatz M, Schape A. Multiresolution segmentation: An optimization approach for high quality multi-scale image segmentation[J]. *Angewandte Geographische Information Sverarbeitung*, 2000(12): 12-23.
- Cui L, Shi J, Ping T, et al. Comparison study on the pixel-based and object-oriented methods of land-use/cover classification with TM data[C].*International Workshop on Earth Observation & Remote Sensing Applications. IEEE*, 2008.
- Feng C., Guo, Y.K. Object-oriented dynamic analysis of road vegetation environment based on remote sensing [J]. *Beijing Surveying and Mapping*, 2016(01):39-42+80. DOI:10.19580/j.cnki.1007-3000.2016.01.010(in Chinese).
- Han C., Zong, L.B, Hu, Y.F., Liu, Z.W., Li, Y.J. Application of UAV remote sensing interpretation in geological hazard investigation of high-voltage transmission lines [J]. *Frontiers in Earth Science*, 2021, 11(6): 835-841.https://doi.org/10.12677/AG.2021.116078(in Chinese).
- Huang C, Wu, L.N., Song, J.L., Yan, X.G. A Comparative Study on Supervised Classification and Object-Oriented Classification of Remote Sensing Images [J]. *Rural Economy and Technology*, 2016,27(23):66-68(in Chinese).
- Ke, J.Y., Lin, Y.J., Tian, P.F., Zhang L. Comparison of optical properties and radiation effects of mixed aerosols at typical sites in East Asia [J]. *Journal of Lanzhou University (Natural Science Edition)*, 2020,56(03):412-421. DOI:10.13885/j.issn.0455-2059. 2020.03.017(in Chinese).
- Kurosaki, Y., Shinoda, M., Mikami, M., 2011. What caused a recent increase in dust outbreaks over East Asia? *Geophys. Res. Lett.* 38, L11702, <http://dx.doi.org/10.1029/2011gl047494>.
- Liu, F.W. Monitoring of Dust Storms on Himawari-8 Satellite Combining Radiation and Timing Information[D].*Shandong University of Science and Technology*, 2018. doi.org/10.27275/d.cn ki.gsdku.2018. 001243(in Chinese).
- Luo, J.N., Xu Z., Qi, Y.G. Global dust remote sensing method based on Fengyun-3 satellite[J].*Journal of Desert Science and Technology*,2015,35(03):690-698(in Chinese).
- Muhammad, A., Sheltami, T.R., Mouftah, H.T., 2012. A review of techniques and technologies for sand and dust storm detection. *Rev. Environ. Sci. Biotechnol.* 11 (3), 305–322. doi.org/ 10.1007/s11157-012-9282-y.
- Qian, W., Leung, J. C.-H., Ren, J., Du, J., Feng, Y., & Zhang, B. (2022). Anomaly based synoptic analysis and model prediction of six dust storms moving from Mongolia to northern China in Spring 2021. *Journal of Geophysical Research: Atmospheres*, 127, e2021JD036272. <https://doi.org/10.1029/2021JD036272>
- Qiao, Y.X., Liu F., Tan, L.Q., Chen T., Mao, H.Y. Object-oriented Forest Land Information Extraction and Classification[J]. *Temperate Forestry Research*, 2019,2(02):25-33(in Chinese).
- Sun, M.D. Research on Dulbert Wetland Change Based on Object-Oriented Classification [D]. China University of Geosciences (Beijing), 2017(in Chinese).
- Twumasi N Y D, Shao Z, Orhan A. Remote sensing and gis methods in urban disaster monitoring and management—an overview[J]. *Int. J. Trend Sci. Res. Dev*, 2019, 3: 918-926. URL: <https://www.ijtsrd.com/papers/ijtsrd23976.pdf>.
- Wang L, and Liu, Q.Y. "Overview of optimal scale selection methods in multi-scale segmentation of high-resolution remote sensing images." *Surveying and Mapping and Spatial Geographic Information* 38.03(2015):166-169(in Chinese).
- Wang, Z.L, Zhu, D.M.Discussion on Maximum Likelihood Classification Algorithm Based on Remote Sensing Image[J].*Henan Science*,2010,28(11):458-461.DOI:10.13537/j.issn.1004-3918.2010.11.030(in Chinese).
- Yang, X.L., Chen L., Zhang, Y.H., Wang, H.L. Diurnal variation characteristics of dust in the eastern Hexi Corridor and its relationship with meteorological factors [J]. *Environmental Science Research*, 2018,31(08):1373-1381. doi.org/10.13198/j.issn.1001-6929.2018.05.10(in Chinese).
- Zhang, B.L. Research Progress on Sand and Dust Weather and Aerosol Effects of Sand and Dust[J]. *Advances in Meteorological Science and Technology*, 2018, 8(1):6 (in Chinese).
- Zhang, H.X., Xu H., Han, D.J, Zheng, F.J, Zhang, W.H. Dynamic sand and dust detection method based on geostationary meteorological satellite[J].*Remote Sensing Information*,2018,33 (01):36-44(in Chinese).
- Zhang L, Zhang L, Du B, et al. Hyperspectral image unsupervised classification by robust manifold matrix factorization[J]. *Information Sciences*, 2019, 485: 154-169. <https://doi.org/10.1016/j.ins.2019.02.00>.